


MOLECULAR AND SYNAPTIC MECHANISMS

Subpopulations of vomeronasal sensory neurons with coordinated coexpression of type 2 vomeronasal receptor genes are differentially dependent on *Vmn2r1*

Sachiko Akiyoshi, Tomohiro Ishii,* Zhaodai Bai and Peter Mombaerts 

Max Planck Research Unit for Neurogenetics, Max-von-Laue-Strasse 4, 60438 Frankfurt, Germany

Keywords: accessory olfactory system, gene expression, gene regulation, pheromone, V2R

Abstract

The mouse vomeronasal organ is specialized in the detection of pheromones. Vomeronasal sensory neurons (VSNs) express chemosensory receptors of two large gene repertoires, *V1R* and *V2R*, which encode G-protein-coupled receptors. Phylogenetically, four families of *V2R* genes can be discerned as follows: A, B, C, and D. VSNs located in the basal layer of the vomeronasal epithelium coordinately coexpress *V2R* genes from two families: Approximately half of basal VSNs coexpress *Vmn2r1* of family C with a single *V2R* gene of family A8-10, B, or D ('C1 type of *V2Rs*'), and the other half coexpress *Vmn2r2* through *Vmn2r7* of family C with a single *V2R* gene of family A1-6 ('C2 type *V2Rs*'). The regulatory mechanisms of the coordinated coexpression of *V2Rs* from two families remain poorly understood. Here, we have generated two mouse strains carrying a knockout mutation in *Vmn2r1* by gene targeting in embryonic stem cells. These mutations cause a differential decrease in the numbers of VSNs expressing a given C1 type of *V2R*. There is no compensatory expression of *Vmn2r2* through *Vmn2r7*. VSN axons coalesce into glomeruli in the appropriate region of the accessory olfactory bulb in the absence of *Vmn2r1*. Gene expression profiling by Nano-String reveals a differential and graded decrease in the expression levels across C1 type of *V2Rs*. There is no change in the expression levels of C2 type of *V2Rs*, with two exceptions that we reclassified as C1 type. Thus, there appears to be a fixed probability of gene choice for a given C2 type of *V2R*.

Introduction

The mouse vomeronasal organ (VNO) is a chemosensory organ residing at the base of the nasal septum that is specialized in the detection of pheromones. Most VSNs express genes of two repertoires that encode chemosensory receptors with a putative seven transmembrane domain structure: vomeronasal receptor genes *V1R* (Dulac & Axel, 1995) and *V2R* (Herrada & Dulac, 1997; Matsunami & Buck, 1997; Ryba & Tirindelli, 1997). The cell bodies of *V1R*⁺ and *V2R*⁺ VSNs reside in the apical and basal layers of the VNO, respectively. The basal layer of VSNs can be subdivided into two sublayers based on the expression of nine non-classical class I major histocompatibility complex genes termed *H2-Mv* (Ishii *et al.*, 2003; Loconto *et al.*, 2003;

Ishii & Mombaerts, 2008; Leinders-Zufall *et al.*, 2014). Axons of VSNs from the apical and basal layers coalesce into multiple glomeruli in the anterior and posterior halves of the accessory olfactory bulb (AOB), respectively (Belluscio *et al.*, 1999; Rodriguez *et al.*, 1999; Del Punta *et al.*, 2002; Ishii & Mombaerts, 2008, 2011).

V2R⁺ VSNs respond physiologically to peptides and proteins (Leinders-Zufall *et al.*, 2004, 2009, 2014; Kimoto *et al.*, 2005; Chamerio *et al.*, 2007, 2011, 2012; Haga *et al.*, 2007, 2010; Sturm *et al.*, 2013). The deduced amino acid sequences of *V2Rs* contain a long N-terminal extracellular region, which may form the ligand-binding site. The mouse genome contains 120 intact *V2R* genes, which can be grouped in four families (A, B, D, and C) based on amino acid sequence homology (Yang *et al.*, 2005; Shi & Zhang, 2007; Young & Trask, 2007; Francia *et al.*, 2014). The largest *V2R* gene family, family A, can be further grouped in nine subfamilies A1 to A10; family A7 exists in rat but not in mouse. Family C, which was originally referred to as *mV2R₂* (Ryba & Tirindelli, 1997) and then mouse *V2R2* (Martini *et al.*, 2001), comprises seven genes in mouse, *Vmn2r1* through *Vmn2r7* (Silvotti *et al.*, 2007, 2011; Francia *et al.*, 2014).

The consensus of numerous *in situ* hybridization (ISH) studies is that mouse family-ABD *V2R* genes are expressed in a punctate and mutually exclusive manner, most likely as a single gene per basal

Correspondence: Peter Mombaerts, as above. E-mail: peter.mombaerts@gen.mpg.de

*Present address: Department of Cell Biology, Graduate School of Medical and Dental Science, Tokyo Medical and Dental University, 1-5-45 Yushima, Bunkyo-ku, Tokyo, 113-8510, Japan

Received 16 November 2017, revised 29 January 2018, accepted 15 February 2018

Edited by C. Giovanni Galizia. Reviewed by Trese Leinders-Zufall, University of Saarland, Germany; Enrique Lanuza, University of Valencia, Spain; and Daisuke Kondoh, Obihiro University of Agriculture and Veterinary Medicine, Japan

All peer review communications can be found with the online version of the article.

VSN. When we knocked out the family-A9 gene *V2rf2/Vmn2r81* and replaced it by the β -galactosidase marker using gene targeting in embryonic stem (ES) cells, we found that ~25% of VSNs that express the marker express another family-ABD *V2R* gene (Ishii & Mombaerts, 2011). This second choice of another family-ABD *V2R* gene can be interpreted in terms of a hypothetical negative feedback mechanism that helps restrict expression of family-ABD *V2R* genes to a single gene per VSN.

In sharp contrast to observations with family-ABD *V2R* genes, ISH probes or antibodies for family-C *V2Rs* label large populations of basal VSNs (Martini *et al.*, 2001; Silvotti *et al.*, 2007, 2011; Ishii & Mombaerts, 2011). Immunoreactive signals with antibodies against family-C members *Vmn2r1* and *Vmn2r2/Vmn2r5* are detected in a mutually exclusive manner, each in approximately half of basal VSNs (Silvotti *et al.*, 2007, 2011). VSNs expressing *V2Rs* of families A8-10, B, and D are preferentially colabeled with anti-*Vmn2r1* antibody, and VSNs expressing *V2Rs* of family A1-6 are preferentially colabeled with *Vmn2r2/Vmn2r5* antibody (Silvotti *et al.*, 2007, 2011). *Vmn2r2* through *Vmn2r7* are coexpressed in various combinations, and many VSNs appear to coexpress all six receptors (Silvotti *et al.*, 2011). Surprisingly, more than twenty years after the discovery of mouse *V2R* genes, there are no reports about mouse strains with a knockout mutation in a family-C gene.

Here, we have generated two novel mouse strains carrying a knockout mutation in *Vmn2r1*. We found that various subpopulations of *V2R*+ VSNs are differentially affected by the absence of *Vmn2r1*; that there is no compensatory expression of *Vmn2r2* through *Vmn2r7*; and that glomeruli form normally if there are sufficient VSNs left. We discovered that *Vmn2r65* (family A5) and *Vmn2r120* (family A6) are C1 type of *V2Rs*, in discordance with their phylogenetic classification as C2 type of *V2Rs*.

Materials and methods

Animal ethics

Mouse studies were carried out in accordance with the German Animal Welfare Act, the European Communities Council Directive 2010/63/EU, and the institutional ethical and animal welfare guidelines of The Rockefeller University, the Max Planck Institute of Biophysics, and the Max Planck Research Unit for Neurogenetics. Approval came from the IACUC of The Rockefeller University, the *Regierungspräsidium* Darmstadt and the *Veterinäramt* of the City of Frankfurt.

Generation of gene-targeted mouse strains

We have previously described the gene-targeted strains *V2r1b-IRES-tauGFP* (Del Punta *et al.*, 2002) and *V2rf2-IRES-tauGFP* (Ishii & Mombaerts, 2011). The internal ribosome entry site sequence (*IRES*) affords bicistronic translation of transcripts. We have here generated four novel mouse strains by gene targeting in the parental ES cell line E14. For the Δ C1 targeting vector, a 2.6 kilobase (kb) upstream fragment and a 4.8 kb downstream fragment flanking exon 1 of the *Vmn2r1* gene were used as the 5' and 3' homologous arms, respectively. The *Hprt* (5')-*loxP-neo* cassette (Ramírez-Solis *et al.*, 1995) was ligated to replace a 1065 basepair (bp) sequence from the *SpeI* site at the 28th nucleotide (nt) before the initiation codon to the *HindIII* site at the 801st nt after the end of exon 1. For the Δ C1-GFP targeting vector, a 2.6 kb upstream fragment and a 5.6 kb downstream fragment of exon 1 of the *Vmn2r1* gene were used as the 5' and 3' homologous arms,

respectively. The *tauGFP-pA* cassette and the self-excising *neo* selectable marker cassette (*ACNF*) were ligated to replace a 230 bp sequence from the initiation codon in-frame to the 4th nt before the end of exon 1. For the *V2rf4-IRES-tauVenus* targeting vector, a 8.2 kb *HpaI-NheI* fragment containing exon 6 of the *Vmn2r83* gene was used to construct the homologous arms. The *IRES-tauVenus-ACNF* cassette was inserted into an *AscI* site that was created one nt after the stop codon of *Vmn2r83*. For the *V2rf1-IRES-taumCherry* targeting vector, a 7.8 kb *SpeI* fragment containing exon 6 of the *Vmn2r82* gene was used to construct the homologous arms. The *IRES-taumCherry-ACNF* cassette was inserted into an artificial *AscI* site one nt after the stop codon of *Vmn2r82*. All DNA sequences for homologous arms were from mouse BAC clones of 129/SvEv genomic origin. The targeting vectors were linearized and electroporated into ES cells as described (Mombaerts *et al.*, 1996). Homologous recombination events were screened and confirmed by Southern blot hybridization with external probes. Cells from gene-targeted ES clones were injected into C57BL/6J blastocysts, and germline transmission was obtained by mating male chimeras with C57BL/6J females. The *ACNF* cassette got removed during transmission through the male germline, leaving a *loxP* sequence behind in the targeted mutation. The strains are publicly available from The Jackson Laboratory in a mixed (129P2/OlaHsd x C57BL/6J) background, as follows: Δ C1 as stock number JR#24643 and strain name B6;129P2-*Vmn2r1*<tm1Mom>/MomJ, Δ C1-GFP as JR#26765 and B6;129P2-*Vmn2r1*<tm2Mom>/MomJ, *V2rf1-mCherry* as JR#7885 and B6;129P2-*Vmn2r82*<tm1Mom>/MomJ, and *V2rf4-Venus* as JR#7886 and B6;129P2-*Vmn2r83*<tm1Mom>/MomJ.

Tissue preparation

Mice were anesthetized by intraperitoneal injection of ketamine and xylazine (210 mg/kg and 10 mg/kg body weight, respectively), and perfused transcardially with phosphate-buffered saline (PBS) at room temperature, followed by ice-cold 4% paraformaldehyde/PBS. The VNO and the brain including the AOB were dissected separately, and post-fixed for 3 h at 4 °C. The samples were then decalcified in 0.45 M EDTA/PBS at 4 °C overnight (for 4-week-old mice) or two nights (for 10-week-old mice), cryoprotected in 15 and 30% sucrose/PBS successively, and frozen in OCT compound (Sakura Finetek #4583). The decalcification step was omitted for brain samples and 0-day-old samples.

Immunohistochemistry and cell counts in the VNO

Coronal 14 μ m cryosections were cut through the entire VNO and collected on glass slides. Sections were treated with 0.5% SDS/PBS for 30 min at room temperature. This step was omitted for *V2Rp5* or GFP IHC alone. After washing with PBS, sections were blocked in 5% normal goat serum (NGS) and 0.3% Triton X-100/PBS, and incubated with primary antibodies in the same blocking solution for 1–2 h at room temperature and then overnight at 4 °C. After washing in 0.1% Triton X-100/PBS, sections were incubated with secondary antibodies and counterstained with DAPI (1:10 000, Invitrogen #D1306) for 2–4 h at room temperature. Primary antibodies and working dilution of each antibody were as follows: rabbit anti-C1 (anti-*Vmn2r1*) antibody (1:500; Silvotti *et al.*, 2007), rabbit anti-C2 (anti-*Vmn2r2/5*) antibody (1:4000; Silvotti *et al.*, 2007), rabbit anti-panC antibody (also referred to as *V2R2*; 1:4000; Martini *et al.*, 2001), rabbit anti-*V2Rp5* antibody (1:1500; Haga *et al.*, 2010), and chicken anti-GFP antibody (1:1500; Aves Labs #GFP-1020). To improve the signal-to-noise ratio of anti-C1, anti-C2, and

anti-GFP IHC, the antibodies were pre-absorbed with acetone powder prepared from brain homogenates of mice with a deletion of the family-C V2R gene cluster generated by genome engineering (Δ V2RCA, unpublished). The antibody solution was incubated with 1% acetone powder overnight at 4 °C, and cleared by centrifugation and filtration before use. The following secondary antibodies were used at 1:1000 dilution: Alexa 488 goat anti-rabbit IgG, Alexa 546 goat anti-rabbit IgG, Alexa 647 goat anti-rabbit IgG, and Alexa 488 goat anti-chicken IgG (Invitrogen #A11034, A11035, A21245, A11039). Sections were examined under a Zeiss LSM 710 confocal microscope without knowing the genotype. Labeled cells were counted on every tenth section (for 4-week and 10-week-old mice) or on every fifth section (for 0-day-old mice). The total cell number per mouse was estimated by multiplying the count by ten or five, respectively. The numbers given are numbers of VSN cell profiles, but for the sake of simplicity, they are referred to as numbers of VSNs.

IHC of the AOB

Serial sagittal 25 μ m sections of the AOB were cut and collected in PBS. To visualize the glomerular layer, free-floating sections were blocked in 5% NGS and 0.2% Tween 20/PBS, and incubated with rabbit anti-VGLUT2 antibody (1:3000; Synaptic Systems #135403) in the same blocking solution for 1–2 h at room temperature, and then overnight at 4 °C. After washing in 0.1% Tween 20/PBS, sections were incubated with Alexa 546 goat anti-rabbit IgG (1:1000) and counterstained with DAPI (1:10 000) for 2–4 h at room temperature. Sections were mounted on glass slides and examined under a Zeiss LSM 710 confocal microscope. For visualization of GFP+ axons, images of the intrinsic fluorescence were taken from serial AOB sections. Multiple sections were aligned using Photoshop, then combined in a z-stacked file using IMAGE J. The 2D images were created by z-projection with maximum intensity method.

NanoString multiplex gene expression analysis

Whole VNO mucosa was dissected in RNA Stabilization Reagent RNAlater (Qiagen #76106). Tissue from a single mouse was placed in a tube and homogenized by TissueLyser LT (Qiagen #85600). Total RNA was extracted using the RNeasy Micro kit with DNase I treatment on the column (Qiagen #74004), and stored at –80 °C until use. A 0.75 μ g aliquot of RNA from each mouse was tested with the custom CodeSet Pao (NanoString Technologies, Seattle, WA, USA). Samples from six wild-type mice and six homozygous mice were analyzed in one cartridge using the nCounter SPRINT Profiler system (NanoString Technologies) according to the manufacturer's instructions. Data processing and statistical analyses were performed using NSOLVER DATA ANALYSIS Software 3.0 (NanoString Technologies). We confirmed that samples passed quality control (QC) criteria based on imaging QC, binding density QC, and positive and negative control probes. We then processed the raw count data into normalized count values in three steps: normalization using a scaling factor calculated from the geometric mean of the six positive control counts, second normalization using a scaling factor calculated from the geometric mean of the counts of four reference genes (*Ano2*, *Cnga4*, *Omp*, *Trpc2*), and background correction by subtracting the mean + 2 standard deviations of eight negative control counts for each sample. Values < 1 after background subtraction were set as 1. Genes with a median count < 100 in wild-type mice were eliminated from further analysis. Changes in gene expression

were estimated by calculating the fold change (FC) of the geometric mean of the counts in mutant mice over the geometric mean of the counts in wild-type mice, and the log₂ FC values were plotted.

In situ hybridization

RNA probes were prepared for the coding sequences of *Vmn2r65* (nt 948–1603 of RefSeq NM_001105180.1), *Vmn2r76* (mix of nt 508–1028 and nt 1219–1590 of RefSeq NM_001102580.1), *Vmn2r118* (nt 822–1306 of RefSeq NM_001104582.1), and *Vmn2r120* (nt 1044–1739 of RefSeq NM_001104591.1; Silvotti *et al.*, 2007). Digoxigenin (DIG) labeling of RNA probes, tissue preparation, and ISH were performed as described previously (Ishii *et al.*, 2004) with some modifications. Coronal 12 μ m sections were cut through the entire VNO, and every 12th section was collected onto a slide for each probe. The incubation time of Proteinase K (Roche #03115828001) was 12 min. Hybridized probes were detected with an alkaline phosphatase-conjugated anti-DIG antibody (1:1000; Roche #11093274910) and BM purple substrate solution (Roche #11442074001). Labeled cells were counted on digital images of sections taken by a Panoramic MIDI slide scanner (3D HISTECH) without knowing the genotype. The total cell number per mouse was determined by multiplying the count by twelve.

ISH combined with IHC

Tissue preparation and ISH were carried out as described above, except that the incubation time of Proteinase K was 5 min. After hybridization and washing, sections were blocked in 5% NGS and 0.3% Triton X-100/PBS, and incubated with alkaline phosphatase-conjugated anti-DIG antibody (1:1000) and anti-C1 antibody (1:500) or anti-C2 antibody (1:4000) in the same blocking solution for two nights at 4 °C. After washing in 0.1% Triton X-100/PBS, sections were incubated with Alexa 488 goat anti-rabbit IgG (1:1000) and DAPI (1:10 000) for 8 h at room temperature. Sections were washed with 0.1% Triton X-100/PBS, and DIG-labeled probes were detected by incubation with HNPP/Fast Red substrate solution (Roche #11758888001) for 30 min. After washing with TN buffer (100 mM Tris pH 7.5, 150 mM NaCl), sections were examined under a Zeiss LSM 710 confocal microscope, directly in TN buffer without mounting.

Experimental design and statistical analysis

For statistical evaluations of cell numbers, the Mann–Whitney test was performed using GRAPHPAD PRISM 5. For NanoString analysis, statistical analysis was performed by NSOLVER DATA ANALYSIS Software 3.0. The false discovery rates (FDR; Benjamini & Yekutieli, 2001) from conducting multiple testing were computed based on the *P*-values of the *t*-test. Genes were considered differentially expressed if FDR < 0.05.

Results

Generation of gene-targeted strains with a knockout mutation in *Vmn2r1*

The mouse V2R gene family C comprises seven intact genes, which are located in a single cluster extending over a 640 kb region on chromosome 3 (Fig. 1A). We generated two mouse strains with a gene-targeted mutation in the *Vmn2r1* gene (referred to as *C1*), which is composed of six coding exons (Fig. 1B).

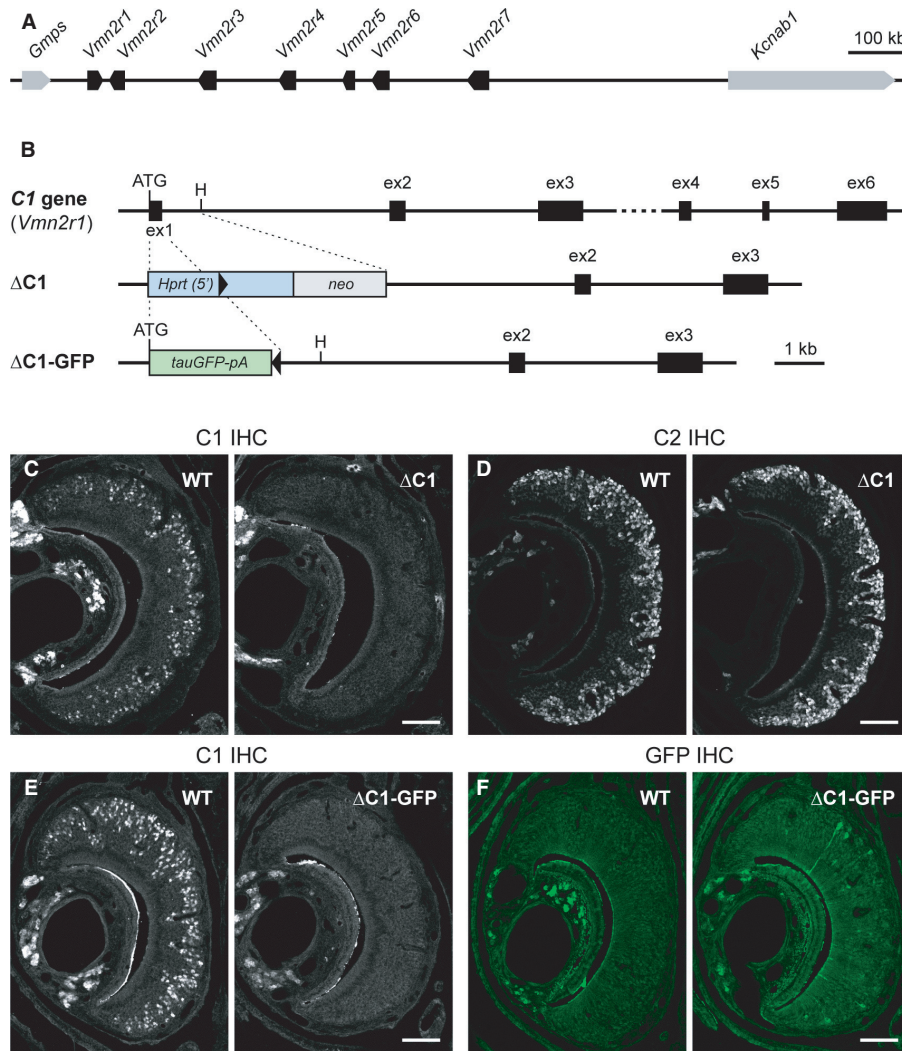


FIG. 1. Generation of mouse strains with a knockout mutation in *Vmn2r1* by gene targeting in ES cells. (A) Genomic organization of the family-C *V2R* genes in mouse. The seven genes *Vmn2r1* through *Vmn2r7* are clustered in a 640 kb region on chromosome 3. The *Vmn2r1* gene is transcribed from the (+) strand, and the other six genes are transcribed from the (-) strand. *Gmps* and *Kcnab1* are the closest genes to the gene cluster, centromerically and telomerically, respectively. (B) Genomic structure and targeted mutagenesis of the family-C gene *Vmn2r1*, abbreviated here as *C1*. This gene is composed of six coding exons. In the $\Delta C1$ strain, a 1065 bp fragment that includes coding exon 1 (ex1) is replaced with a *Hprt(5')*-*loxP*-*neo* cassette. This cassette is left behind in the targeted mutation in the mouse strain. In the $\Delta C1$ -GFP strain, a 230 bp fragment from the initiation *ATG* codon to the fourth nt before the end of coding exon 1 is replaced in frame with a *tauGFP-pA* cassette, followed by a self-excising *neo* selectable marker cassette (*ACNF*). Following the removal of *ACNF*, one *loxP* site is left behind in the targeted mutation in the mouse strain, after *tauGFP-pA*. The black triangles indicate a *loxP* site. H, *HindIII*. (C,D) IHC with anti-C1 antibody (C) and anti-C2 antibody (D) on coronal sections of the VNO from wild-type (WT) and homozygous ($\Delta C1$) mice of the $\Delta C1$ strain. Mice were male and 10 weeks old. There is no C1 immunoreactivity in $\Delta C1$ mice (C), and no obvious difference in C2 immunoreactivity between WT and $\Delta C1$ mice (D). Scale bar, 100 μ m. (E,F) IHC with anti-C1 antibody (E) and anti-GFP antibody (F) on coronal sections of the VNO from WT and homozygous ($\Delta C1$ -GFP) mice of the $\Delta C1$ -GFP strain. Mice were male and 4 weeks old. There is no C1 immunoreactivity in $\Delta C1$ -GFP mice (E). Sparse GFP+ cells are detected in $\Delta C1$ -GFP mice (F). Scale bar, 100 μ m.

In the first strain ($\Delta C1$), we replaced a 1065 bp sequence including coding exon 1 with a selectable marker cassette. Immunohistochemistry (IHC) with anti-C1 antibody revealed immunoreactivity in the basal layer of the VNO in wild-type mice (WT) but not in homozygous (hereafter referred to as $\Delta C1$) mice (Fig. 1C). The anti-C1 antibody is called 'anti-*Vmn2r1* antibody' in Silvotti *et al.* (2007), and recognizes the antigen peptide region encoded by exons 3 and 4. The absence of C1 immunoreactivity in $\Delta C1$ mice confirms that the C1 mutation is a null mutation, and that no truncated C1 protein is produced. The anti-C2 antibody is called 'anti-*Vmn2r2* antibody' in Silvotti *et al.* (2007), and recognizes both *Vmn2r2* and *Vmn2r5* (Silvotti *et al.*, 2007, 2011). We found no obvious difference in C2 immunoreactivity between WT and $\Delta C1$ mice (Fig. 1D),

indicating that the selection marker that is left in the targeted mutation does not disturb the expression of the neighboring genes.

In the second strain ($\Delta C1$ -GFP), we replaced a 230 bp sequence of exon 1 with a *tauGFP-pA* cassette. Here too, there is no C1 immunoreactivity in homozygous mice ($\Delta C1$ -GFP), consistent with the null design of the targeted mutation (Fig. 1E). The *tauGFP* marker fused to the initiation codon should enable us to detect VSNs in which the mutant *C1* locus is transcribed, but no functional C1 receptor is expressed. However, we observed only sparse GFP+ VSNs in $\Delta C1$ -GFP mice. The intrinsic GFP fluorescence in VSNs of $\Delta C1$ -GFP mice was weak and needed to be enhanced by IHC with anti-GFP antibody (Fig. 1F). The number of GFP+ VSNs in $\Delta C1$ -GFP mice and in mice heterozygous for this mutation (data not

shown) is much less than the number of VSNs detected by anti-C1 antibody in WT mice. The mutant allele may yield unstable transcripts; alternatively, transcription of the mutant allele may extinguish with time.

We established the $\Delta C1$ and $\Delta C1$ -GFP strains in a mixed (129P2/OlaHsd \times C57BL/6J) background. We maintained the strains by mating heterozygous mice, such that WT and homozygous mice were obtained from the same litters. $\Delta C1$ mice and $\Delta C1$ -GFP mice are viable and fertile and show no obvious differences in appearance compared to their WT littermates. These strains are publicly available from The Jackson Laboratory.

Differential and graded decrease in the numbers of VSNs that express C1 type of V2R genes

We examined the effects of the $\Delta C1$ mutation on the numbers of various subpopulations of V2R+ VSNs in the VNO.

First, we crossed the $\Delta C1$ strain with the gene-targeted strains V2r1b-IRES-tauGFP (abbreviated as V2r1b-GFP; Del Punta *et al.*, 2002) or V2rf2-IRES-tauGFP (abbreviated as V2rf2-GFP; Ishii & Mombaerts, 2011). In these strains, VSNs that express the *V2r1b/Vmn2r26* gene (family B, C1 type) or the *V2rf2/Vmn2r81* gene (family A9, C1 type), respectively, coexpress tauGFP by virtue of IRES-mediated bicistronic translation. We have previously shown that >90% of V2r1b-GFP+ VSNs and V2rf2-GFP+ VSNs are colabeled with anti-C1 antibody, and rarely with anti-C2 antibody (Ishii & Mombaerts, 2011). We counted GFP+ VSNs on VNO sections of $\Delta C1$ mice and their WT littermates in crosses of $\Delta C1$ with V2r1b-GFP or V2rf2-GFP. We observed a marked decrease in the number of V2r1b-GFP+ VSNs in $\Delta C1$ mice (Fig. 2A). At 4 week, the number of V2r1b-GFP+ VSNs was decreased to 21.5% of WT (mean \pm SEM in $\Delta C1$, 185 \pm 16 compared to WT, 860 \pm 76; $n = 4$ per genotype; Mann–Whitney test, $P = 0.0286$) (Fig. 2E). At 10 week, this number was decreased further to 9.5% of WT ($\Delta C1$, 85 \pm 16 compared to WT, 898 \pm 113; $n = 4$ per genotype; $P = 0.0286$) (Fig. 2E). There was no significant difference at 0 day ($\Delta C1$, 490 \pm 35 compared to WT, 391 \pm 24; $n = 4$ per genotype; $P = 0.0571$); we counted V2r1b-GFP+ VSNs stained by anti-GFP antibody, as the intrinsic GFP fluorescence was weak in WT and $\Delta C1$ at 0 day (Fig. 2B,E). The subpopulation of V2rf2-GFP+ VSNs was also affected in $\Delta C1$ mice, but to a different extent and with a different time course than the subpopulation of V2r1b-GFP+ VSNs: at 4 weeks, the number was not significantly different ($\Delta C1$, 2033 \pm 184 compared to WT, 2093 \pm 154; $n = 4$ per genotype; $P = 0.8857$), and at 10 weeks, it was decreased to 63.4% of WT ($\Delta C1$, 585 \pm 50 compared to WT, 923 \pm 43; $n = 4$ per genotype; $P = 0.0294$) (Fig. 2C,E). The anti-V2Rp5 antibody labels VSNs that express the *Vmn2r116* gene, which belongs to family A3 (Haga *et al.*, 2010). Consistent with the preferential colabeling of family-A3 V2Rs with anti-C2 antibody (Silvotti *et al.*, 2007, 2011), we found that the majority of V2Rp5+ VSNs was colabeled with anti-C2 antibody (190 of 261, 72.8%) and rarely with anti-C1 antibody (2 of 287, 0.7%). Accordingly, we found no significant difference in the number of V2Rp5+ VSNs between WT mice and $\Delta C1$ mice at 10 weeks ($\Delta C1$, 2375 \pm 429 compared to WT, 2450 \pm 387; $n = 4$ per genotype; $P = 0.8857$) (Fig. 2D,E). Figure 2E shows a summary of VSN counts, and the differential and graded effects of the $\Delta C1$ mutation on subpopulations of V2R+ VSNs. The numbers of V2r1b-GFP+ and V2rf2-GFP+ VSNs, which were colabeled with anti-C1 antibody but not with anti-C2 antibody, were decreased in $\Delta C1$ mice with age and to different extents, and the numbers of V2Rp5+ VSNs, which

were colabeled with anti-C2 antibody but not with anti-C1 antibody, were not affected in $\Delta C1$ mice.

Using the same design as for the V2r1b-GFP and V2rf2-GFP strains, we next generated two gene-targeted strains called V2rf4-Venus and V2rf1-mCherry. We inserted *IRES-tauVenus* and *IRES-taumCherry* after the stop codon of the *V2rf4/Vmn2r83* and *V2rf1/Vmn2r82* genes, respectively (Fig. 3A). These two genes belong to family A9, a family of four C1 type of V2Rs: *V2rf1/Vmn2r82*, *V2rf2/Vmn2r81*, *V2rf3/Vmn2r80*, *V2rf4/Vmn2r83*. We found that, indeed, V2rf4-Venus+ VSNs and V2rf1-mCherry+ VSNs were colabeled preferentially with anti-C1 antibody (93 of 123, 76% and 22 of 38, 58%, respectively), but not with anti-C2 antibody (0 of 140 and 0 of 40, respectively). In $\Delta C1$ mice at 10 weeks, the number of V2rf4-Venus+ VSNs was decreased to 15.5% of WT ($\Delta C1$, 208 \pm 28 compared to WT, 1345 \pm 82; $n = 4$ per genotype; $P = 0.0286$) (Fig. 3B), and the number of V2rf1-mCherry+ VSNs was decreased to 35.5% of WT ($\Delta C1$, 285 \pm 32 compared to WT, 803 \pm 67; $n = 4$ per genotype; $P = 0.0286$) (Fig. 3C). In $\Delta C1$ -GFP mice at 10 weeks, the number of V2rf1-mCherry+ VSNs was decreased to 35.8% of WT ($\Delta C1$ -GFP, 263 \pm 17 compared to WT, 733 \pm 117; $n = 4$ per genotype; $P = 0.0286$) (Fig. 3D). Thus, the two mutations in *Vmn2r1* had the same effect on the subpopulation of V2rf1-mCherry+ VSNs (Fig. 3E).

In summary, the *Vmn2r1* mutations affect differentially the four populations of C1 type of V2R+ VSNs that we examined with gene-targeted strains of the V2R-IRES-marker design. At 10 weeks, V2r1b-GFP+ VSNs and V2rf4-Venus+ VSNs were strongly affected (decreased to 9.5 and 15.5% of WT, respectively), and V2rf2-GFP+ VSNs and V2rf1-mCherry+ VSNs were less affected (decreased to 63.4 and 35.5% of WT, respectively).

No compensatory expression of other family-C V2R genes

Conceivably, other members of family-C V2Rs may become expressed in the C1 type of V2R+ VSNs that remain in $\Delta C1$ and $\Delta C1$ -GFP mice. Such expression might occur to compensate for the loss of C1 receptor function and as a result of the absence of a hypothetical negative feedback, analogous to what we observed in V2rf2 knockout mice (Ishii & Mombaerts, 2011).

To test this possibility, we examined coexpression of other family-C V2Rs in C1 type of V2R+ VSNs by immunohistochemistry with anti-C2 antibody. Representative images of VNO sections from 10-week-old mice with intrinsic signal of the fluorescent marker and C2 immunoreactivity are shown for the crosses $\Delta C1 \times V2rf2$ -GFP (Fig. 4A) and $\Delta C1 \times V2rf1$ -mCherry (Fig. 4B). Only a few V2rf2-GFP+ VSNs (4 of 369, 1%) and V2rf1-mCherry+ VSNs (5 of 321, 2%) were colabeled with anti-C2 antibody in WT mice, consistent with the preferential colabeling with anti-C1 antibody. In $\Delta C1$ mice, the colabeling percentages with anti-C2 antibody in V2rf2-GFP+ VSNs (2 of 234, 1%) and V2rf1-mCherry+ VSNs (3 of 114, 3%) were equally low. Likewise, in the cross $\Delta C1$ -GFP \times V2rf1-mCherry (Fig. 4C), V2rf1-mCherry+ VSNs were rarely colabeled with the anti-C2 antibody in WT mice (2 of 293, 1%) and in $\Delta C1$ -GFP mice (4 of 105, 4%). Figure 4D shows the summary of colabeling analysis in 10-week-old mice (data from 4 mice per genotype for each cross) including the results for V2r1b-GFP+ and V2rf4-Venus+ VSNs. We found no compensatory expression of *Vmn2r2* and *Vmn2r5* (as detected with anti-C2 antibody) in these VSNs in the absence of C1 expression.

The anti-C2 antibody does not detect *Vmn2r3*, *Vmn2r6*, and *Vmn2r7* (Silvotti *et al.*, 2011). We further examined the possibility

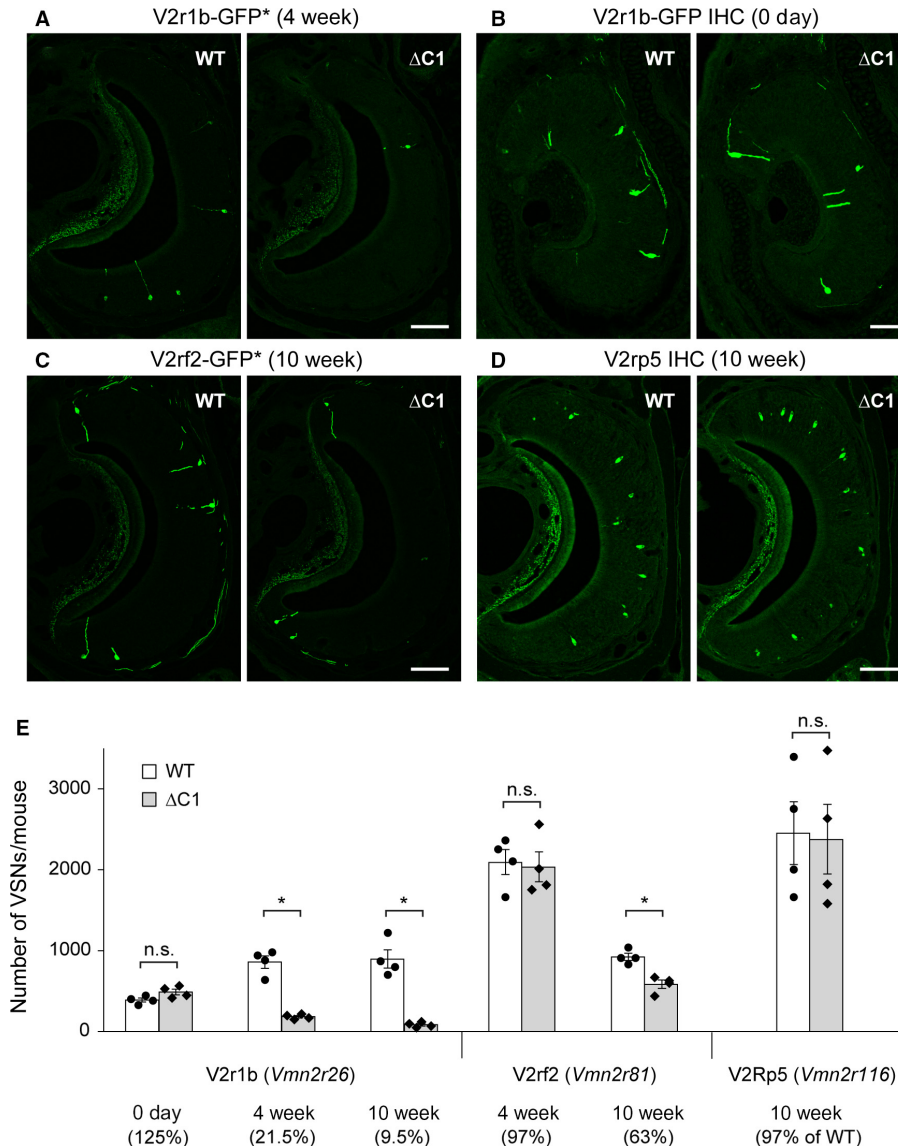


FIG. 2. Decrease in the number of VSNS expressing V2r1b-GFP or V2rf2-GFP but not Vmn2r116 in $\Delta C1$ mice. (A–C) The $\Delta C1$ strain was crossed with the gene-targeted V2r1b-GFP and V2rf2-GFP strains to generate double-homozygous mice. Intrinsic GFP fluorescence (indicated with an asterisk) of coronal VNO sections is shown in A,C. IHC with anti-GFP antibody is shown in B. Scale bar, 100 μm in A,C, and 50 μm in B. (D) IHC with anti-V2Rp5 antibody on coronal VNO sections from WT and $\Delta C1$ mice. Scale bar, 100 μm . (E) Summary of the numbers of labeled VSNS per mouse. Four mice per genotype were analyzed for each cross at the indicated ages. Mice were male, except for 0 day, when both males and females were used. Error bars represent mean \pm SEM, with data points superimposed on bar charts. Mann–Whitney test was performed: n.s., not significant; * P value < 0.05 .

of compensatory expression of other members of family-C V2Rs using an anti-panC antibody (Fig. 4E–H), which recognizes all seven family-C V2Rs (Martini *et al.*, 2001; Silvotti *et al.*, 2007). In WT mice, large fractions of V2r1b-GFP+, V2rf2-GFP+, V2rf4-Venus+, and V2rf1-mCherry+ VSNS were colabeled with panC antibody at 10 weeks, reflecting the preferential coexpression of Vmn2r1 in these VSNS, respectively, 87.8, 79.1, 75.2, and 74.6 or 72.7%. In sharp contrast, these subpopulations of VSNS were rarely colabeled with panC antibody in $\Delta C1$ and $\Delta C1$ -GFP mice, respectively, 3, 1, 2, 5, or 4% (data from 4 mice per genotype for each cross).

Taken together, we found no evidence for compensatory expression of other family-C V2Rs in the absence of Vmn2r1. The subpopulations of C1 type of V2R+ VSNS that we examined do not appear to express any functional family-C receptor.

Axonal projections of subpopulations of VSNS in $\Delta C1$ mice

V2R+ VSNS project their axons to the pAOB, where they coalesce into multiple glomeruli. V2r1b-GFP+ glomeruli are located in the anterior part of the pAOB (Del Punta *et al.*, 2002; Ishii & Mombaerts, 2008), and V2rf2-GFP+ glomeruli in the middle part of the pAOB (Ishii & Mombaerts, 2011; Leinders-Zufall *et al.*, 2014). Deletion of the V2rf2 gene results in a diffuse distribution of axons across the pAOB (Ishii & Mombaerts, 2011).

As a first step in elucidating possible biological functions of Vmn2r1, we asked if it is required for axonal wiring of VSNS that express C1 type of V2Rs. We examined the intrinsic GFP fluorescence in AOB sections of 4-week-old mice from the crosses $\Delta C1 \times V2r1b$ -GFP and $\Delta C1 \times V2rf2$ -GFP. We found that $\Delta C1$ mice had only a few and small V2r1b-GFP+ glomeruli

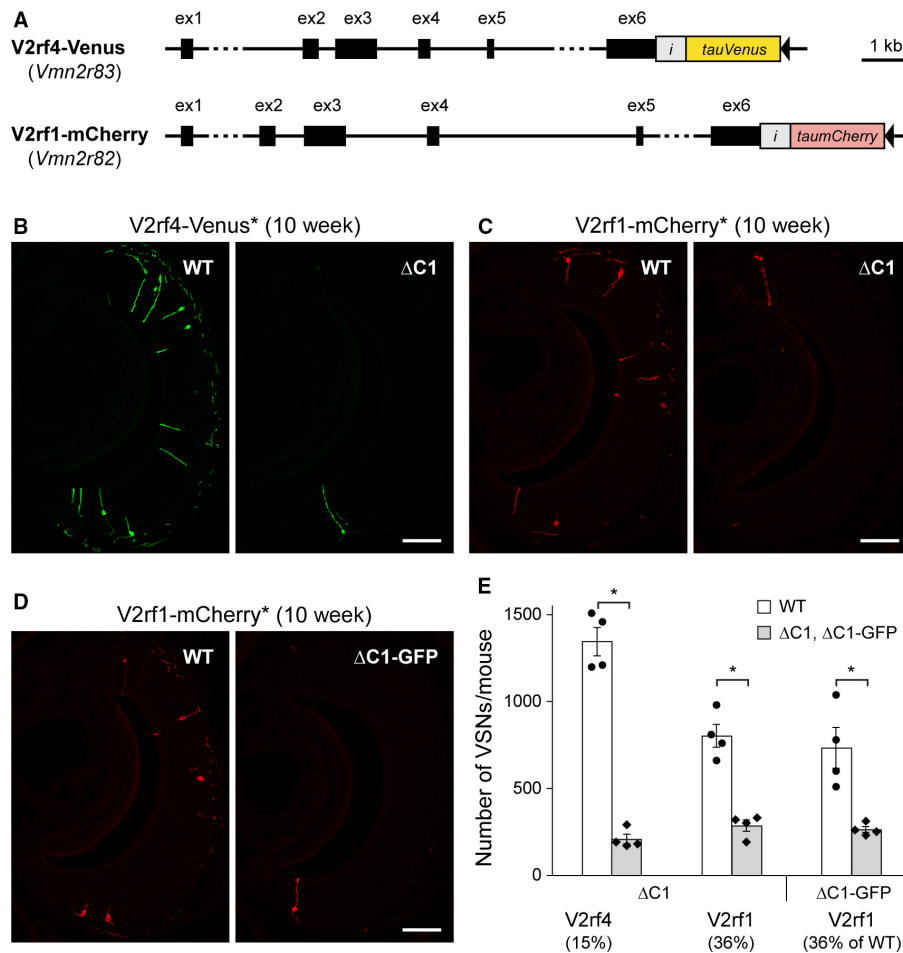


FIG. 3. Decrease in the number of VSNS expressing V2rf4-Venus or V2rf1-mCherry in Δ C1 mice. (A) The V2rf4-Venus and V2rf1-mCherry gene-targeted strains have an insertion of *IRES-tauVenus* or *IRES-taumCherry* after the stop codon of the *Vmn2r83* or *Vmn2r82* genes, respectively. The coding sequences remain intact. The black triangles indicate a *loxP* site. *i*, IRES. (B,C) The Δ C1 strain was crossed with the V2rf4-Venus and V2rf1-mCherry strains to generate double-homozygous mice. Intrinsic fluorescence (indicated with an asterisk) of coronal VNO sections is shown in green (B) or red (C). Scale bar, 100 μ m. (D) The Δ C1-GFP strain was crossed with the V2rf1-mCherry strain to generate double-homozygous mice. Intrinsic fluorescence of coronal VNO sections is shown in red. Scale bar, 100 μ m. (E) Summary of the numbers of labeled VSNS per mouse. Four 10-week-old male mice per genotype were analyzed for each cross. Error bars represent mean \pm SEM, with data points superimposed on bar charts. Mann-Whitney test was performed: **P* value < 0.05.

(Fig. 5A), consistent with a decrease in the number of V2r1b-GFP+ VSNS at 4 weeks to 21.5% of WT (Fig. 2E). The small glomeruli in Δ C1 mice resided in the anterior part of pAOB, where V2r1b-GFP+ axons normally coalesce. We then visualized the glomerular layer of AOB, where VSN axons terminate and form synaptic connections, by IHC for a presynaptic marker using an anti-VGLUT2 antibody. We found that the few and small V2r1b-GFP+ glomeruli in Δ C1 mice were located in the VGLUT2+ glomerular layer, as was the case in WT mice (Fig. 5B). But for V2rf2-GFP+ VSNS, which were not affected in Δ C1 mice at 4 weeks (97% of WT, Fig. 2E), we observed multiple glomeruli with strong GFP intensity in the middle part of the pAOB in WT and Δ C1 mice, and without obvious difference in the pattern (Fig. 5C).

Thus, *Vmn2r1* appear not to be required for the guidance of axons of V2rf2-GFP+ VSNS from the VNO to the appropriate region of the AOB, and for the formation of V2rf2 glomeruli. This finding excludes a major biological function of *Vmn2r1* in axonal wiring and coalescence.

Gene expression profiling by NanoString multiplex analysis

The NanoString platform enables multiplex analysis of RNA levels of large gene repertoires such as *ORs* and *VRs* with high specificity

and sensitivity (Khan *et al.*, 2011, 2013; Leinders-Zufall *et al.*, 2014). We designed a custom CodeSet Pao consisting of probes to analyze *V2R* gene expression in Δ C1 and Δ C1-GFP mice. Specific probes against the coding sequences were designed for 45 *V2R* genes, which is one-third of the repertoire of 120 *V2R* genes. To obtain higher coverage, we designed additional probes against 3' UTR sequences for 24 *V2R* genes, based on the sequence data from a transcriptome study by RNA-seq in the mouse VNO (Ibarra-Soria *et al.*, 2014). We were unable to design specific NanoString probes for family-A4 *V2Rs* due to the high sequence homology among the family members. Of 69 *V2R* probes in CodeSet Pao, 10 probes gave very low counts in 10-week-old WT mice. Genes with a median count < 100 in WT samples were considered as not expressed in whole VNO mucosa at the age of analysis, and deleted from data. Of the probes designed against 3'UTR sequences, two gave extraordinary high counts; they were considered as non-specific, and these data were also deleted from the analysis. CodeSet Pao thus enabled us to examine expression of 57 *V2R* genes, covering 48% of the *V2R* gene repertoire and all *V2R* families except for family A4.

We examined total RNA samples from whole VNO mucosae of individual 10-week-old mice from the Δ C1 and Δ C1-GFP strains.

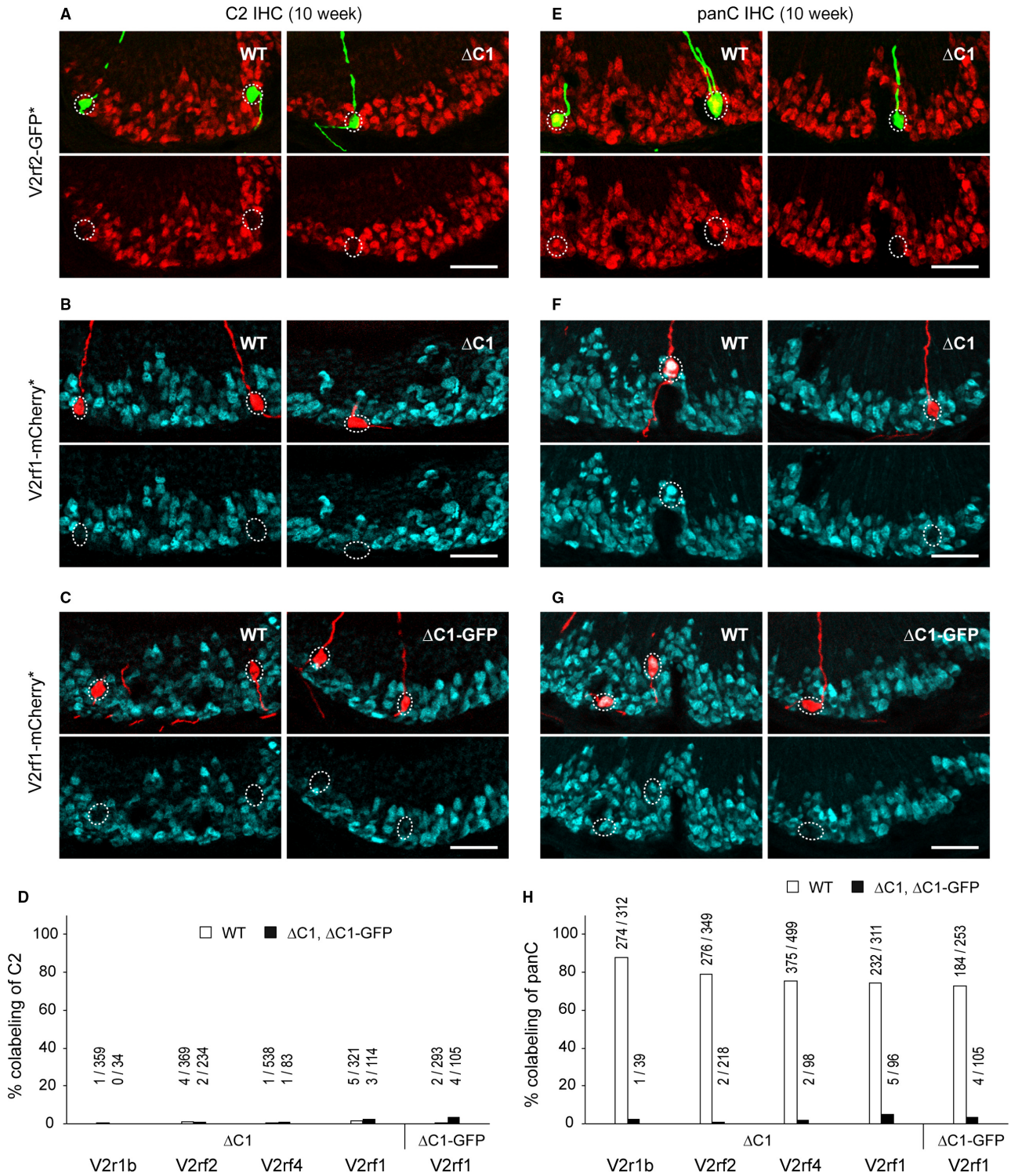


FIG. 4. No compensatory expression of *Vmn2r2* through *Vmn2r7* in the absence of *Vmn2r1*. (A,B) IHC with anti-C2 antibody on coronal VNO sections of WT and $\Delta C1$ mice from the crosses $\Delta C1 \times V2rf2$ -GFP (A) and $\Delta C1 \times V2rf1$ -mCherry (B). In (A) intrinsic GFP fluorescence (indicated with an asterisk) is shown in green, and C2 immunoreactivity in red. In (B) intrinsic mCherry fluorescence is shown in red, and C2 immunoreactivity in blue. Mice were male and 10 weeks old. Scale bar, 50 μm . (C) IHC with anti-C2 antibody on coronal VNO sections of WT and $\Delta C1$ mice from the crosses $\Delta C1$ -GFP \times *V2rf1*-mCherry at 10 weeks. Intrinsic mCherry fluorescence is shown in red. Scale bar, 50 μm . (D) Summary of the percentage of colabeling with anti-C2 antibody in VSNs that express a fluorescence marker from a gene-targeted locus. Four mice per genotype were analyzed for each cross. Samples were from the 10-week-old male mice that were used for VSN counting in Figs 2 and 3. Above each bar, the number of double-labeled VSNs/number of fluorescence marker-positive VSNs is given. (E,F) IHC with anti-panC antibody on coronal VNO sections of WT and $\Delta C1$ mice from the crosses $\Delta C1 \times V2rf2$ -GFP (E) and $\Delta C1 \times V2rf1$ -mCherry (F) at 10 weeks. In (E) intrinsic GFP fluorescence is shown in green, and panC immunoreactivity in red. In (F) intrinsic mCherry fluorescence is shown in red, and panC immunoreactivity in blue. Scale bar, 50 μm . (G) IHC with anti-panC antibody (blue) on coronal VNO sections of WT and $\Delta C1$ -GFP mice from the cross $\Delta C1$ -GFP \times *V2rf1*-mCherry at 10 weeks. Intrinsic mCherry fluorescence is shown in red. Scale bar, 50 μm . (H) Summary of the percentage of colabeling with panC antibody in fluorescence marker-expressing VSNs. Four 10-week-old male mice per genotype were analyzed for each cross.

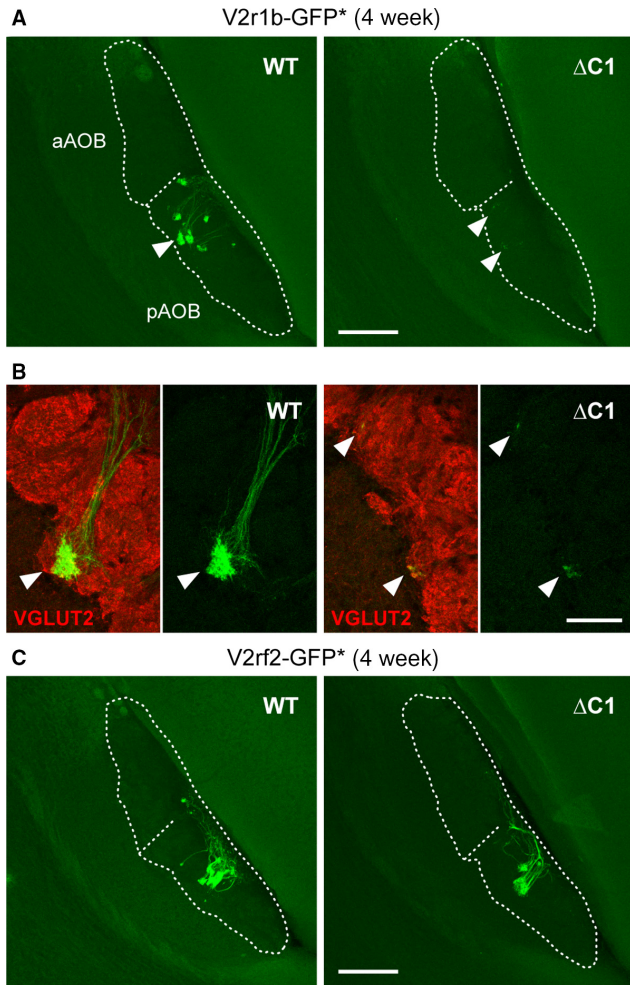


FIG. 5. Axonal projections of subpopulations of VSNS to the AOB. (A) Axonal projections of V2r1b-GFP+ VSNS to the AOB of WT and $\Delta C1$ mice from the cross $\Delta C1 \times V2r1b-GFP$. Samples were from 4-week-old male and female mice. Multiple images of intrinsic GFP fluorescence from serial sagittal sections were z-stacked and projected into a 2D image. Dashed lines indicate the contours of the nerve layer and the glomerular layer of the AOB, and the border between the anterior AOB (aAOB) and the posterior AOB (pAOB). Arrowheads indicate GFP+ glomeruli (WT) and GFP+ axons ($\Delta C1$) that are shown in B. Scale bar, 200 μm . (B) IHC with anti-VGLUT2 antibody (red) on sagittal AOB sections of WT and $\Delta C1$ mice from the cross $\Delta C1 \times V2r1b-GFP$, combined with intrinsic GFP fluorescence. Arrowheads V2r1b-GFP+ glomeruli in WT, and GFP+ axons terminating in the VGLUT2+ glomerular layer in $\Delta C1$. Scale bar, 50 μm . (C) Axonal projections of V2rf2-GFP+ VSNS to the AOB in WT and $\Delta C1$ mice from the cross $\Delta C1 \times V2rf2-GFP$. Samples were from 4-week-old female mice. Axons with intrinsic GFP fluorescence form multiple glomeruli of various sizes in the pAOB both in WT and $\Delta C1$ mice. Scale bar, 200 μm .

Six WT mice and six homozygous (MUT) mice were analyzed for each strain. Differential expression between WT and MUT mice was evaluated by the false discovery rates (FDR) based on the P -value of the Student's t -test for each gene. If FDR is < 0.05 , a gene was considered differentially expressed (DE). Counts for *Vmn2r1* were at background level in MUT mice of the $\Delta C1$ and $\Delta C1$ -GFP strains, confirming that these gene-targeted mutations are null mutations.

Figure 6A plots the \log_2 of the fold change (FC) of the mean count in MUT mice over the mean count in WT mice for the 57 V2R genes, arranged in order of gene families from C, A1–10, B, to D. Comparison of the results from $\Delta C1$ and $\Delta C1$ -GFP strains revealed that there were no significant differences between the two

strains: Gene expression profiles of V2R genes were very similar between the strains, as shown by close \log_2 FC values and overlap of the 99% confidence intervals (CI) for each gene. Only a few genes showed a discrepancy: *Vmn2r94* and *Vmn2r104* are non-DE genes in the data from the $\Delta C1$ strain, whereas these genes were markedly decreased in the data from the $\Delta C1$ -GFP strain. An explanation is that for both *Vmn2r94* and *Vmn2r104*, counts in the corresponding WT samples were substantially lower in the $\Delta C1$ strain than in the $\Delta C1$ -GFP strain, resulting in differences of \log_2 FC values between the strains. The differences in counts in WT samples for *Vmn2r94* and *Vmn2r104* may reflect the mixed genetic background of the $\Delta C1$ and $\Delta C1$ -GFP strains.

Family-ABD V2Rs are classified into two groups according to the colabeling patterns with antibodies against family-C V2Rs (Silvotti *et al.*, 2011). V2Rs of family-A1 to A6 are preferentially colabeled with anti-C2 antibody, and appear to coexpress *Vmn2r2* through *Vmn2r7* (C2 type of V2Rs). V2Rs of family-A8, A9, A10, B, and D are preferentially colabeled with anti-C1 antibody and coexpress *Vmn2r1* (C1 type of V2Rs). Of the 26 C1 type of V2Rs analyzed with CodeSet Pao (the right side of the diagram in Fig. 6A), 24 showed a significant decrease in MUT mice of the $\Delta C1$ and $\Delta C1$ -GFP strains; of these 24, 19 were DE in both strains, and the remaining 5 were DE in one but not the other strain (Fig. 6A). In sharp contrast, there was no difference in expression of 25 of the 27 C2 type of V2R genes analyzed with CodeSet Pao (the left side of the diagram in Fig. 6A). This analysis is consistent with the differential effects of the *Vmn2r1* mutations on the various subpopulations of VSNS that express C1 type of V2Rs. We identified two exceptions: *Vmn2r65* of family-A5 and *Vmn2r120* of family-A6 were significantly decreased in MUT mice. *Vmn2r5* of family-C is the only gene that was increased in MUT mice in both strains.

The NanoString results are highly consistent with the cell counts on VNO sections (Fig. 6B, data from 10-week-old mice were used for the comparison). *Vmn2r81/V2rf2* gave lower NanoString counts in $\Delta C1$ and $\Delta C1$ -GFP mice, but the FC values were not significantly different; interestingly, the \log_2 FC values in NanoString were close to the \log_2 values of the ratio of the number of V2rf2-GFP+ VSNS in MUT over WT mice. *Vmn2r83/V2rf4* showed a significant decrease in NanoString analysis, and to the same extent as the decrease of the number of V2rf4-Venus+ VSNS in cell counts. There was no difference in *Vmn2r116* expression or in the number of V2Rp5+ VSNS.

CodeSet Pao includes probes for the nine non-classical major histocompatibility *H2-Mv* genes that are expressed in V2R+ VSNS (Ishii *et al.*, 2003; Loconto *et al.*, 2003; Ishii & Mombaerts, 2008; Leinders-Zufall *et al.*, 2014). We found that *H2-M1* and *H2-M9* counts were decreased significantly in $\Delta C1$ and $\Delta C1$ -GFP mice; *H2-M9* was DE in both strains, *H2-M1* was DE in one strain (Fig. 6C). The other *H2-Mv* genes were not affected. The decrease in *H2-Mv* gene expression level is consistent with the preferential expression of *H2-M10* genes in VSNS colabeled with anti-C2 antibody (Silvotti *et al.*, 2007), the coexpression of *H2-M9* with *V2rf1-3* genes (Ishii *et al.*, 2003; Ishii & Mombaerts, 2008), and the decreased number of V2rf2-GFP+ VSNS and V2rf1-mCherry+ VSNS.

Reclassification of *Vmn2r65* and *Vmn2r120* as C1 type of V2R genes

Studies with family-specific antibodies have classified families A5 and A6 as C2 type of V2Rs (Silvotti *et al.*, 2007, 2011). Our

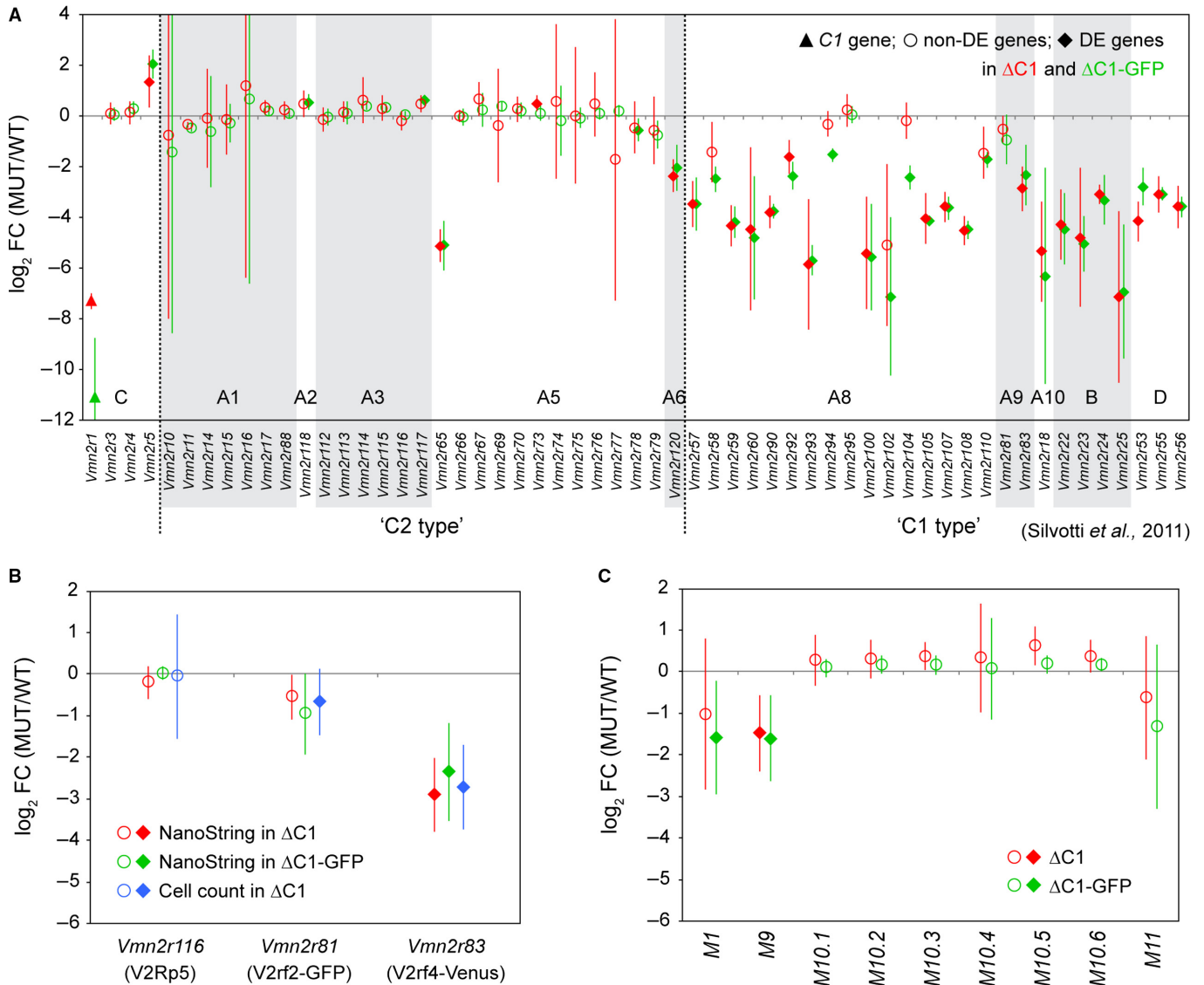


FIG. 6. NanoString multiplex gene expression analysis of total RNA from whole VNO mucosae. (A) Gene expression profiling of *V2R* genes by NanoString analysis with the custom CodeSet Pao for strains ΔC1 (red) and ΔC1-GFP (green). Six WT and six homozygous (MUT) mice were analyzed for each strain. Mice were 10-week-old males. The log₂ values of the fold change (FC) of MUT over WT are plotted. Filled triangles indicate the *Vmn2r1/C1* gene: Its NanoString count in MUT mice is near background level. Filled diamonds indicate differentially expressed (DE) genes, with a false discovery rate (FDR) < 0.05. Open circles indicate non-DE genes. Columns are alternatively gray-shaded and not shaded per gene family. Expression profiles are very similar between two strains, as shown by similar log₂ FC values and overlap of error bars (±99% CI). (B) NanoString results in strains ΔC1 (red) and ΔC1-GFP (green) are consistent with differences in cell counts in the ΔC1 strain (blue). Filled diamonds indicate DE genes in NanoString analysis or a significant decrease in cell count. Open circles indicate non-DE genes. Error bars represent log₂ FC ±99% CI. (C) Gene expression profiling of *H2-Mv* genes by NanoString analysis with CodeSet Pao in strains ΔC1 (red) and ΔC1-GFP (green). Filled diamonds indicate DE genes. Open circles indicate non-DE genes. Error bars represent log₂ FC ±99% CI. Expression profiles are very similar between the two strains.

NanoString results, however, indicate that counts for *Vmn2r65* (family A5) and *Vmn2r120* (family A6) were decreased significantly in ΔC1 and ΔC1-GFP mice. To follow up on these unexpected NanoString results, we performed ISH analyses using gene-specific probes for *Vmn2r65* and *Vmn2r120*, and counted the numbers of labeled VSNs on VNO sections from 10-week-old mice of the ΔC1-GFP strain (Fig. 7A,B). In ΔC1-GFP mice, the number of *Vmn2r65*⁺ VSNs was decreased to 5.7% of WT (ΔC1-GFP, 87 ± 8 compared to WT, 1515 ± 108; *n* = 4 per genotype; Mann–Whitney test, *P* = 0.0294), and the number of *Vmn2r120*⁺ VSNs was decreased to 37.0% of WT (ΔC1-GFP, 615 ± 82 compared to WT, 1662 ± 153; *n* = 4 per genotype; *P* = 0.0284). As a control

experiment, we tested *Vmn2r118* (family A2) and *Vmn2r76* (family A5). These are non-DE genes in NanoString analysis, and they also showed no changes in ISH cell counts in ΔC1-GFP mice: *Vmn2r118* in ΔC1-GFP, 816 ± 47 compared to WT, 744 ± 27 (*n* = 4 per genotype; *P* = 0.2454), and *Vmn2r76* in ΔC1-GFP, 1545 ± 129 compared to WT, 1650 ± 108 (*n* = 4 per genotype; *P* = 0.6857). A comparison of NanoString and ISH results validates the concordance in the differences for these four *V2R* genes (Fig. 7C).

Finally, we examined the coexpression patterns by ISH using gene-specific probes in combination with IHC using anti-C1 and anti-C2 antibodies, in three 10-week-old WT C57BL/6J mice (Fig. 7D–G). We found that the majority of *Vmn2r65*⁺ VSNs

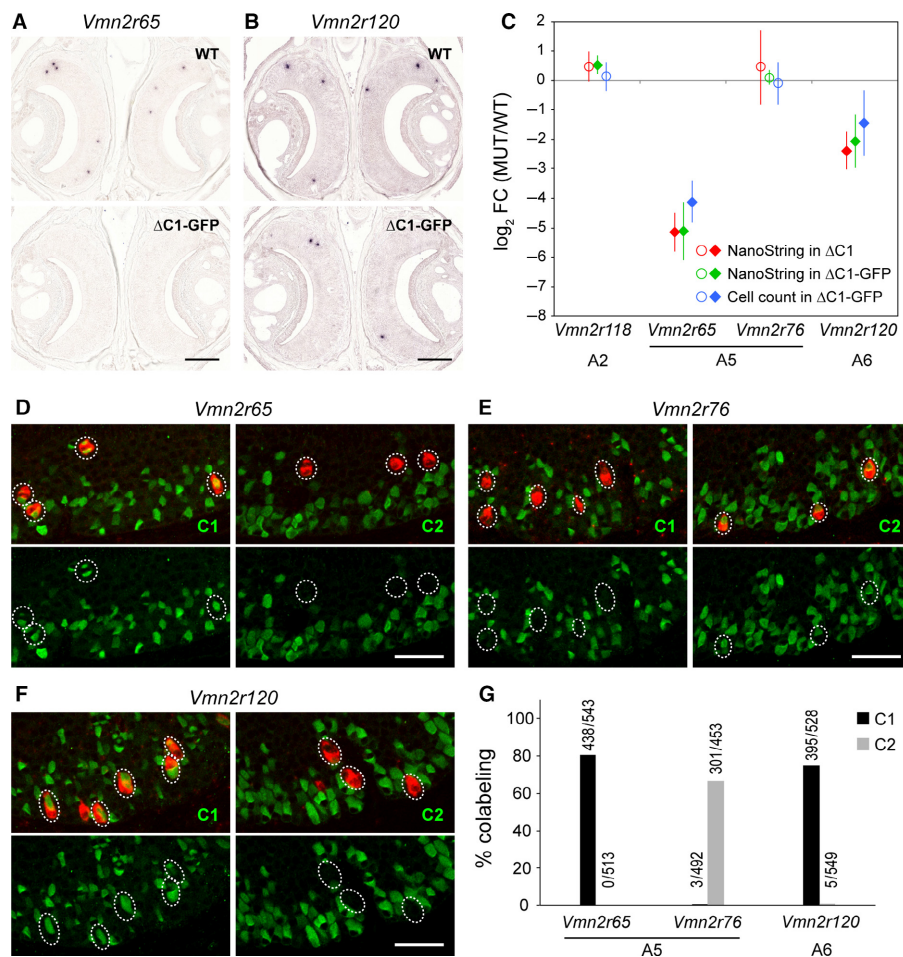


FIG. 7. Reclassification of *Vmn2r65* and *Vmn2r120* as C1 type of V2R genes. (A,B) ISH with gene-specific probes for *Vmn2r65* (A) and *Vmn2r120* (B) on coronal VNO sections of WT and Δ C1-GFP mice. Labeled cells were visualized chromogenically. Four 10-week-old male mice per genotype were used. Scale bar, 200 μ m. (C) Comparison of NanoString counts with ISH cell counts. Filled diamonds indicate DE genes in NanoString analysis or a significant decrease in cell count by ISH. Open circles indicate non-DE genes. *Vmn2r65* and *Vmn2r120* were decreased in MUT mice consistently in NanoString and ISH analyses, and to the same extent for each gene: The \log_2 FC values are close, and there is overlap of the error bars ($\pm 99\%$ CI). By contrast, there was no difference in ISH counts using gene-specific probes for *Vmn2r118* and *Vmn2r76* genes, consistent with NanoString results. (D–F) Colabeling of *Vmn2r65* (D), *Vmn2r76* (E), and *Vmn2r120* (F) by fluorescence ISH (red) in combination with IHC using anti-C1 or anti-C2 antibodies (green) on coronal VNO sections of C57BL/6J mice at 10 weeks. Scale bar, 50 μ m. (G) Summary of the combined ISH/IHC analysis. VNO sections from three 10-week-old C57BL/6J male mice were analyzed. Above each bar, the number of double-labeled VSNS/number of VSNS labeled by ISH with a gene-specific probe is shown. The majority of VSNS expressing *Vmn2r65* or *Vmn2r120* in ISH were colabeled with C1 antibody, thus reclassifying these genes as C1 type of V2Rs.

(family A5) were colabeled with anti-C1 antibody (438 of 543, 81%), and none were colabeled with the anti-C2 antibody (0 of 513, 0%). In contrast, a large fraction of *Vmn2r76*+ VSNS (also family A5) was colabeled with anti-C2 antibody (301 of 453, 66%), and a few were colabeled with anti-C1 antibody (3 of 492, 1%). The NanoString CodeSet Pao contains probes for 12 of the 15 family-A5 V2R genes, and of these 12, only *Vmn2r65* was affected by the *Vmn2r1* mutation. This phenotype is readily explained by the coexpression patterns: family-A5 V2Rs are colabeled with anti-C2 antibody, but *Vmn2r65* is an exception. As *Vmn2r120* is the sole gene in family-A6, the ISH probe is likely to be specific to *Vmn2r120*. We found that the majority of *Vmn2r120*+ VSNS were colabeled with anti-C1 antibody (395 of 528, 74.8%), and few *Vmn2r120*+ VSNS were colabeled with anti-C2 antibody (5 of 549, 1%).

Taken together, the histological analyses validate the apparent exceptions in the NanoString results, and lead us to reclassify *Vmn2r65* and *Vmn2r120* firmly as C1 type of V2Rs, in discordance with their phylogenetic classification as C2 type of V2Rs.

Discussion

Sequential and dependent model of coordinated coexpression of V2R genes

We have here described mouse strains with a knockout mutation in the *Vmn2r1* gene, twenty years after mouse V2R genes were reported (Matsunami & Buck, 1997; Ryba & Tirindelli, 1997). The anti-C1 and anti-C2 antibodies (Silvotti *et al.*, 2007, 2011) were critical reagents for our study, as gene-specific ISH probes for family-C genes have proved difficult to design.

A first insight into the regulatory mechanisms of the coordinated expression of a single family-ABD gene with one or more family-C genes came from our analysis of a mouse strain with a gene-targeted deletion of the coding sequence of *V2rf2* (Ishii & Mombaerts, 2011). We found that $\sim 25\%$ of VSNS that express the mutant *V2rf2* allele coexpress another family-ABD gene, consistent with the absence of a hypothetical negative feedback from the mutant *V2rf2* allele. Interestingly, 9.5% of VSNS expressing the mutant *V2rf2* allele were colabeled with anti-C2 antibody, vs. 0% of *V2rf2*-GFP+

VSNs. We have proposed a sequential and dependent model for the coordinated expression of two *V2R* genes: a family-ABD gene is expressed first during differentiation of a VSN, and then the appropriate family-C gene(s) is/are expressed next, in a dependent manner (Ishii & Mombaerts, 2011). The lack of compensatory expression of family-C genes in VSNs expressing C1 type of *V2Rs* in the absence of *Vmn2r1* is consistent with our sequential and dependent model.

Differential and graded dependence of V2R+ VSN subpopulations on Vmn2r1

We analyzed the impact of a *Vmn2r1* knockout mutation on various subpopulations of VSNs that express C1 type of *V2Rs* in three complementary ways: by cell counts in crosses of Δ C1 and Δ C1-GFP with gene-targeted strains carrying *V2R* mutations of the IRES-marker design, by cell counts using ISH with *V2R* gene-specific probes, and by RNA counts with the NanoString multiplex gene expression platform. The four available gene-targeted strains carrying *V2R* mutations of the IRES-marker design provide the highest degree of analytical specificity for cell counting: V2r1b-IRES-tauGFP (Del Punta *et al.*, 2002), V2rf2-IRES-tauGFP (Ishii & Mombaerts, 2011), V2rf4-IRES-tauVenus and V2rf1-IRES-taumCherry (this paper). The number of marker-positive VSNs in the Δ C1 or Δ C1-GFP background was reduced to 9.5, 63.4, 15.5, 35.5, or 35.8% of WT, respectively. By ISH with *V2R* gene-specific probes, we found that the number of VSNs was reduced to 5.7% for *Vmn2r65* and 37.0% for *Vmn2r120*. These decreases in cell counts correlate remarkably well with the FC values in the NanoString analysis, which reflect expression levels measured in total, non-reverse transcribed RNA from whole VNO mucosa. Assuming that these correlations can be generalized to other family-ABD genes, the FC values in the NanoString analysis can thus be converted into reductions in cell numbers. The number of presumptive VSNs expressing a given C1 type of *V2R* would then be reduced to an average of 21.83% of WT in Δ C1 and 15.13% in Δ C1-GFP, and to a median of 7.68% of WT in Δ C1 and 8.04% in Δ C1-GFP. Interestingly, V2r1b+ VSNs and V2rf4+ VSNs are *H2-Mv-* and were affected much more than V2rf2+ VSNs and V2rf1+ VSNs, which are *H2-Mv+* (Ishii & Mombaerts, 2008). Further work is needed to determine whether subpopulations of *H2-Mv-* VSNs are reduced to a greater extent than *H2-Mv+* VSNs in the absence of *Vmn2r1*, and what the effects would be of eliminating *H2-Mv* expression completely by generating double mutants with our Δ H2Mv strain (Leinders-Zufall *et al.*, 2014).

Subpopulations of VSNs that express C2 type of *V2R* genes are not dependent on *Vmn2r1*, suggesting cell-autonomous effects of the *Vmn2r1* knockout mutations. By IHC analysis, we found no significant difference in the number of V2Rp5+ VSNs. By NanoString analysis, we found no significant difference in expression of 25 of the 27 C2 type of *V2Rs*; the two C2 type of *V2Rs* that were DE (*Vmn2r65* and *Vmn2r120*) could be reclassified as C1 type of *V2R* genes. By ISH analysis, there was no significant difference in cell counts for C2 type of *V2R* genes *Vmn2r118* and *Vmn2r76*.

Varying percentages of colabeling with anti-C1 antibody and varying reductions in the Δ C1 or Δ C1-GFP background

Not all VSNs expressing a given C1 type of *V2R* are colabeled with anti-C1 antibody; the colabeling is preferential, not absolute. The percentage of colabeling at 10 weeks was 58% for V2rf1 (in V2rf1-mCherry mice), 74.8% for *Vmn2r120* (in C57BL6/J mice), 76% for

V2rf4 (in V2rf4-Venus mice), 80.7% for *Vmn2r65* (ISH in C57BL6/J mice), 91.1% for V2rf2 (in V2rf2-GFP mice, Ishii & Mombaerts, 2011), and 93% for V2r1b (in V2r1b-GFP mice, Ishii & Mombaerts, 2011). There could be differences in sensitivity of the analytical techniques and fluorescent markers used, but the general conclusion is that most—but not all—VSNs of a subpopulation expressing a given C1 type of *V2R* coexpress *Vmn2r1*. At 3 weeks, this percentage of colabeling is lower (Ishii & Mombaerts, 2011): 68.2% for V2rf2 (in V2rf2-GFP mice), and 81.3% for V2r1b (in V2r1b-GFP mice). We speculate that with increasing age, a higher fraction of existing VSNs may start to coexpress *Vmn2r1*, perhaps as final maturation or induction by an activity-dependent mechanism. An alternative, but not mutually exclusive hypothesis, is that with increasing age, *Vmn2r1-* VSNs get replaced by *Vmn2r1+* VSNs during the continuous process of cell death and neurogenesis in the vomeronasal epithelium.

As not all VSNs of a subpopulation of expressing a C1 type of *V2R* are colabeled with anti-C1 antibody in WT mice, and the percentage of colabeling varies among C1 type of *V2Rs*, it is not surprising that the reductions of C1 type of *V2Rs* in the Δ C1 or Δ C1-GFP background were not complete, and varied. But, there is no correlation between the percentage of colabeling in WT mice and the percentage of reduction in the Δ C1 or Δ C1-GFP background. Therefore, the simple explanation cannot be offered that there would be two subsets for each C1 type of *V2R+* VSN subpopulation: a subset of VSNs that normally express *Vmn2r1* and do not survive in the absence of *Vmn2r1*, and a subset of VSNs that never express *Vmn2r1* and survive in the absence of *Vmn2r1*.

Possible functions of Vmn2r1

The observation of few and small glomeruli formed by axons of V2r1b+ VSNs in the absence of *Vmn2r1* is consistent with the high reduction in cell number. A minimal number of olfactory sensory neurons expressing a given odorant receptor is required to maintain glomeruli in the olfactory bulb (Ebrahimi & Chess, 2000). Nonetheless, some axons of V2r1b+ VSNs reach the glomerular layer. Importantly, axons of V2rf2+ VSNs formed normal glomeruli in the appropriate region of the AOB, consistent with the lower reduction in cell number compared to V2r1b+ VSNs. These findings exclude a major biological function for *Vmn2r1* in axon guidance from the VNO to the AOB, and in the coalescence of axons into glomeruli.

Results from a heterologous HEK293 expression system suggest that *Vmn2r1* is a calcium-dependent, low-sensitivity receptor for isoleucine, leucine, and valine (DeMaria *et al.*, 2013). If these responses can be extended *in vivo* or *ex vivo* to VSNs of WT mice and can be shown to be reduced or abolished in the Δ C1 or Δ C1-GFP background, the reduced cell number could be interpreted in terms of reduced VSN survival due to absent or aberrant physiological responses. *Vmn2r1* may respond to its own ligands, such as amino acids, independently of the family-ABD receptor responding to, for instance, peptides (Leinders-Zufall *et al.*, 2009, 2014). *Vmn2r1* may promote surface expression of a family-ABD receptor in native VSNs, as suggested by studies in the heterologous HEK293 system (DeMaria *et al.*, 2013).

Reclassification of Vmn2r65 and Vmn2r120 as C1 type of V2R genes

An unexpected observation in the NanoString analysis was that *Vmn2r65* and *Vmn2r120* were DE, although they were thought to

be C2 type of V2Rs based on their phylogenetic classification in families A5 and A6, respectively. This analysis turned out to have predictive power. We found that the numbers of VSNs expressing *Vmn2r65* and *Vmn2r120* were reduced in Δ C1-GFP mice, and to the same extent as the reduction in NanoString counts. We then showed that VSNs expressing *Vmn2r65* and *Vmn2r120* were colabeled preferentially with anti-C1 antibody but rarely with anti-C2 antibody in C57BL6/J mice. We have thus reclassified *Vmn2r65* and *Vmn2r120* firmly as C1 type of V2Rs. Application of RNA-seq may result in the reclassification of more V2Rs.

Conclusion

Subpopulations of VSNs expressing C2 type of V2Rs are not upregulated in the absence of *Vmn2r1*; they do not appear to 'fill the void' created by the decrease in VSN subpopulations expressing C1 type of V2Rs. There thus appears to be a fixed probability of gene choice for a given C2 type of V2R, resulting in subpopulations of C2 type of V2R+ VSNs that are tightly regulated in terms of cell numbers.

Acknowledgements

The authors are grateful to Dr. Roberto Tirindelli and Dr. Kazushige Touhara for gifts of antibodies. P.M. thanks the Max Planck Society for generous financial support. The gene-targeted strains V2rf1-IRES-taumCherry and V2rf4-IRES-tauVenus were generated by T.I. in the laboratory of P.M. at The Rockefeller University, New York, NY.

Conflict of interest

The authors have no financial or other relationships to report that might lead to a conflict of interest.

Data accessibility

Original data are available upon request from the corresponding author. The NanoString probe sequences and data have been deposited in the Gene Expression Omnibus (NCBI) and are accessible by GEO accession number GSE104703.

Author contributions

S.A. and P.M. designed research, reviewed data, and wrote the manuscript. S.A., T.I., and Z.B. performed research.

Abbreviations

AOB, accessory olfactory bulb; CI, confidence intervals; DE, differentially expressed; DIG, digoxigenin; ES, embryonic stem; FC, fold change; FDR, false discovery rate; IHC, immunohistochemistry; *IRES*, internal ribosome entry site; ISH, *in situ* hybridization; NGS, normal goat serum; PBS, phosphate-buffered saline; VNO, vomeronasal organ; VSNs, vomeronasal sensory neurons.

References

Belluscio, L., Koentges, G., Axel, R. & Dulac, C. (1999) A map of pheromone receptor activation in the mammalian brain. *Cell*, **97**, 209–220.
 Benjamini, Y. & Yekutieli, D. (2001) The control of the false discovery rate in multiple testing under dependency. *Ann. Stat.*, **29**, 1165–1188.
 Chamero, P., Marton, T.F., Logan, D.W., Flanagan, K., Cruz, J.R., Saghatelian, A., Cravatt, B.F. & Stowers, L. (2007) Identification of protein pheromones that promote aggressive behaviour. *Nature*, **450**, 899–902.
 Chamero, P., Katsoulidou, V., Hendrix, P., Bufe, B., Roberts, R., Matsunami, H., Abramowitz, J., Birnbaumer, L. *et al.* (2011) G protein *G α*

is essential for vomeronasal function and aggressive behavior in mice. *Proc. Natl. Acad. Sci. USA*, **108**, 12898–12903.
 Chamero, P., Leinders-Zufall, T. & Zufall, F. (2012) From genes to social communication: molecular sensing by the vomeronasal organ. *Trends Neurosci.*, **35**, 597–606.
 Del Punta, K., Puche, A., Adams, N.C., Rodriguez, I. & Mombaerts, P. (2002) A divergent pattern of sensory axonal projections is rendered convergent by second-order neurons in the accessory olfactory bulb. *Neuron*, **35**, 1057–1066.
 DeMaria, S., Berke, A.P., Van Name, E., Heravian, A., Ferreira, T. & Ngai, J. (2013) Role of a ubiquitously expressed receptor in the vertebrate olfactory system. *J. Neurosci.*, **33**, 15235–15247.
 Dulac, C. & Axel, R. (1995) A novel family of genes encoding putative pheromone receptors in mammals. *Cell*, **83**, 195–206.
 Ebrahimi, F.A.W. & Chess, A. (2000) Olfactory neurons are interdependent in maintaining axonal projections. *Curr. Biol.*, **10**, 219–222.
 Francia, S., Silvotti, L., Ghirardi, F., Catzeflis, F., Percudani, R. & Tirindelli, R. (2014) Evolution of spatially coexpressed families of type-2 vomeronasal receptors in rodents. *Genome Biol. Evol.*, **7**, 272–285.
 Haga, S., Kimoto, H. & Touhara, K. (2007) Molecular characterization of vomeronasal sensory neurons responding to a male-specific peptide in tear fluid: sexual communication in mice. *Pure Appl. Chem.*, **79**, 775–783.
 Haga, S., Hattori, T., Sato, T., Sato, K., Matsuda, S., Kobayakawa, R., Sakano, H., Yoshihara, Y. *et al.* (2010) The male mouse pheromone ESP1 enhances female sexual receptive behavior through a specific vomeronasal receptor. *Nature*, **466**, 118–122.
 Herrada, G. & Dulac, C. (1997) A novel family of putative pheromone receptors in mammals with a topographically organized and sexually dimorphic distribution. *Cell*, **90**, 763–773.
 Ibarra-Soria, X., Levitin, M.O., Saraiva, L.R. & Logan, D.W. (2014) The olfactory transcriptomes of mice. *PLoS Genet.*, **10**, e1004593.
 Ishii, T. & Mombaerts, P. (2008) Expression of nonclassical class I major histocompatibility genes defines a tripartite organization of the mouse vomeronasal system. *J. Neurosci.*, **28**, 2332–2341.
 Ishii, T. & Mombaerts, P. (2011) Coordinated coexpression of two vomeronasal receptor V2R genes per neuron in the mouse. *Mol. Cell Neurosci.*, **46**, 397–408.
 Ishii, T., Hirota, J. & Mombaerts, P. (2003) Combinatorial coexpression of neural and immune multigene families in mouse vomeronasal sensory neurons. *Curr. Biol.*, **13**, 394–400.
 Ishii, T., Omura, M. & Mombaerts, P. (2004) Protocols for two- and three-color fluorescent RNA *in situ* hybridization of the main and accessory olfactory epithelia in mouse. *J. Neurocytol.*, **33**, 657–669.
 Khan, M., Vaes, E. & Mombaerts, P. (2011) Regulation of the probability of mouse odorant receptor gene choice. *Cell*, **147**, 907–921.
 Khan, M., Vaes, E. & Mombaerts, P. (2013) Temporal patterns of odorant receptor gene expression in adult and aged mice. *Mol. Cell Neurosci.*, **57**, 120–129.
 Kimoto, H., Haga, S., Sato, K. & Touhara, K. (2005) Sex-specific peptides from exocrine glands stimulate mouse vomeronasal sensory neurons. *Nature*, **437**, 898–901.
 Leinders-Zufall, T., Brennan, P., Widmayer, P., Chandramani, P.S., Maul-Pavicic, A., Jager, M., Li, X.H., Breer, H. *et al.* (2004) MHC class I peptides as chemosensory signals in the vomeronasal organ. *Science*, **306**, 1033–1037.
 Leinders-Zufall, T., Ishii, T., Mombaerts, P., Zufall, F. & Boehm, T. (2009) Structural requirements for the activation of vomeronasal sensory neurons by MHC peptides. *Nat. Neurosci.*, **12**, 1551–1558.
 Leinders-Zufall, T., Ishii, T., Chamero, P., Hendrix, P., Oboti, L., Schmid, A., Kircher, S., Pyrski, M. *et al.* (2014) A family of nonclassical class I MHC genes contributes to ultrasensitive chemodetection by mouse vomeronasal sensory neurons. *J. Neurosci.*, **34**, 5121–5133.
 Loconto, J., Papes, F., Chang, E., Stowers, L., Jones, E.P., Takada, T., Kumanovics, A., Lindahl, K.F. *et al.* (2003) Functional expression of murine V2R pheromone receptors involves selective association with the M10 and M1 families of MHC class Ib molecules. *Cell*, **112**, 607–618.
 Martini, S., Silvotti, L., Shirazi, A., Ryba, N.J. & Tirindelli, R. (2001) Co-expression of putative pheromone receptors in the sensory neurons of the vomeronasal organ. *J. Neurosci.*, **21**, 843–848.
 Matsunami, H. & Buck, L.B. (1997) A multigene family encoding a diverse array of putative pheromone receptors in mammals. *Cell*, **90**, 775–784.
 Mombaerts, P., Wang, F., Dulac, C., Chao, S.K., Nemes, A., Mendelsohn, M., Edmondson, J. & Axel, R. (1996) Visualizing an olfactory sensory map. *Cell*, **87**, 675–686.

- Ramírez-Solis, R., Liu, P. & Bradley, A. (1995) Chromosome engineering in mice. *Nature*, **378**, 720–724.
- Rodríguez, I., Feinstein, P. & Mombaerts, P. (1999) Variable patterns of axonal projections of sensory neurons in the mouse vomeronasal system. *Cell*, **97**, 199–208.
- Ryba, N.J. & Tirindelli, R. (1997) A new multigene family of putative pheromone receptors. *Neuron*, **19**, 371–379.
- Shi, P. & Zhang, J. (2007) Comparative genomic analysis identifies an evolutionary shift of vomeronasal receptor gene repertoires in the vertebrate transition from water to land. *Genome Res.*, **17**, 166–174.
- Silvotti, L., Moiani, A., Gatti, R. & Tirindelli, R. (2007) Combinatorial co-expression of pheromone receptors, V2Rs. *J. Neurochem.*, **103**, 1753–1763.
- Silvotti, L., Cavalca, E., Gatti, R., Percudani, R. & Tirindelli, R. (2011) A recent class of chemosensory neurons developed in mouse and rat. *PLoS One*, **6**, e24462.
- Sturm, T., Leinders-Zufall, T., Maček, B., Walzer, M., Jung, S., Pömmerl, B., Stevanović, S., Zufall, F. *et al.* (2013) Mouse urinary peptides provide a molecular basis for genotype discrimination by nasal sensory neurons. *Nat. Commun.*, **4**, 1616.
- Yang, H., Shi, P., Zhang, Y.P. & Zhang, J. (2005) Composition and evolution of the V2r vomeronasal receptor gene repertoire in mice and rats. *Genomics*, **86**, 306–315.
- Young, J.M. & Trask, B. (2007) V2R gene families degenerated in primates, dog and cow, but expanded in opossum. *Trends Genet.*, **23**, 212–215.